Surface & Coatings Technology 309 (2017) 54–58

Contents lists available at ScienceDirect

Surface & Coatings Technology

journal homepage: www.elsevier.com/locate/surfcoat

The effect of heat treatment on structural and electronic properties of niobium nitride prepared by a thermal diffusion method

Ashraf Hassan Farha [a,b,*], Osman Murat Ozkendir [c], Hani E. Elsayed-Ali [a], Ganapati Myneni [d], Yüksel Ufuktepe [e,*]

[a] Department of Electrical and Computer Engineering, The Applied Research Center, Old Dominion University, Norfolk, VA 23529, USA
[b] Department of Physics, Faculty of Science, Ain Shams University, Cairo 11566, Egypt
[c] Tarsus Technology Faculty, Mersin University, Tarsus 33480, Turkey
[d] Thomas Jefferson National Accelerator Facility, Newport News, VA 23606, USA
[e] Department of Physics, Cukurova University, Adana, 01330, Turkey

ARTICLE INFO

Article history:
Received 23 August 2016
Revised 5 November 2016
Accepted in revised form 13 November 2016
Available online 15 November 2016

Keywords:
NbN_x
Nitride
Surface morphology
XRD
Thermal diffusion
XAS

ABSTRACT

Niobium nitride (NbN_x) coatings were prepared onto Nb substrate by thermal diffusion at high temperatures. The formation of NbN_x coating by thermal diffusion was studied in the range of 1250–1500 °C at constant nitrogen background gas pressure (1.3×10^{-3} Pa) and processing time (180 min). The electronic and crystal structures of the NbN_x coatings were investigated. It was found that nitrogen diffuses into Nb forming the Nb-N solid solution (bcc) α-NbN phase that starts to appear above 1250 °C. Increasing the processing temperature gives richer α-phase concentration. Besides, X-ray absorption spectroscopy (XAS) was performed to study the electronic structure of the NbN_x layer. The results of the electronic structural study corroborate the crystal structural analysis. The Nb $M_{3,2}$ edge X-ray absorption spectroscopy (XAS) spectrum shows strong temperature dependence. At the highest processing temperature (1500 °C), the number of *d* holes increased. Electrostatic interaction between *d* electron and core hole was increased due to nitrogen diffusion into the niobium. For the studied conditions, only the α-NbN was observed in the X-ray diffraction patterns.

© 2016 Elsevier B.V. All rights reserved.

1. Introduction

Niobium nitride (NbN_x) is considered a promising material for many technical and industrial applications. Attractive physical and chemical properties of NbN_x, such as high superconducting transition temperature (T_c ~ 17.3 K), strong wear resistance, thermal and chemical stabilities, and high hardness make it useful for many applications. Most of the applications of NbN_x are related to its superconductivity properties, such as using of NbN_x layer as a diffusion barrier in Josephson junctions [1,2], coating of superconducting cables, single photon detectors [3], and hot electron bolometers [4,5].

Different preparation methods have been employed to grow NbN_x thin films, such as metal-organic chemical vapor deposition MOCVD [6], dc and rf sputtering [7,8], ion beam assisted deposition (IBAD) [9], and pulsed laser deposition (PLD) [10,11]. There are different types of substrates that were used for the growth of NbN_x films. MgO and sapphire substrates were used for growth of NbN_x films with NaCl structure (δ-NbN phase) because of the small lattice mismatch (about 10%) between these substrates and the δ-NbN phase [12]. Other works were done to prepare NbN_x films on Nb substrates for good mechanical properties of the films. In our previous studies, the hexagonal β-Nb_2N phase showed higher stress and hardness than the cubic δ-NbN phase [13]. NbN_x films grown on Nb substrates at different PLD conditions were studied for their nanomechanical and crystal structural properties [13,14].

Nitriding of bulk Nb substrates can be achieved by the so-called reactive diffusion method [15–19] or combustion synthesis [20]. NbN_x thin films were also produced using rapid thermal processing by heating of Nb thin films deposited on Si in molecular nitrogen or ammonia [21,22]. In general, these methods depend on adsorption of nitrogen or ammonia gas at the surface of the Nb substrate that is heated at high temperatures, then it diffuses into Nb and forms NbN_x. The treatment of Nb samples at different conditions (heating temperature, nitrogen background pressure, and heating time and rate) results in samples with diverse properties. The reactive diffusion process has advantages to nitride deposition that include: being less expensive, easy to apply, and covering lager areas, and resulting in a relatively thick nitride with homogenous thickness within a short processing time [17]. Theoretical works predict good performances of NbN_x, if it replaces Nb in superconducting applications of rf cavities [23]. Several experimental works were done using thermal diffusion method to study the formation of NbN_x for possible usages in superconducting rf cavities [17,23–26].

* Corresponding authors at: Department of Physics, Cukurova University, Adana, 01330, Turkey.
E-mail addresses: ahass006@odu.edu (A.H. Farha), ufuk@cu.edu.tr (Y. Ufuktepe).

http://dx.doi.org/10.1016/j.surfcoat.2016.11.044
0257-8972/© 2016 Elsevier B.V. All rights reserved.

Benvenuti et al. [23]., studied the formation of niobium nitride by reactive diffusion at 1270–1500 °C and nitrogen pressure in the range of 10^3-10^5 Pa. In their work, they studied the influence of heating time and nitriding pressure and temperature on the critical phase transition temperatures of the NbN_x β, γ and δ phases. As they reported, applying higher temperatures or longer process times resulted in poorer quality films. Also, nitriding should be carried out at 10^5 Pa and 1380 °C or higher for more than 6 min to get higher T_c value.

Fabbricatore et al. [24]. reported on using nitrogen diffusion at nitrogen pressures and temperature in the range of $10^4-3\times10^4$ Pa and 1000–2000 °C, respectively. NbN_x films with mixed phases were obtained. Temperatures below 1300 °C gave only the β and α phases. The γ, δ and ε phases were identified as the processing temperatures was increased to 1300 °C and above. Tu et al. [25] reported that thermal diffusion of nitrogen into bulk Nb at 800 °C gives samples with surface resistance lower than that of pure Nb by 2–3 times. To the best of our knowledge, there are no published reports on the diffusion mechanism of nitrogen in Nb substrate at the lower gas pressure of 1.3×10^{-3} Pa. On the other hand, the mechanisms of nitrogen diffusion into Nb were reported for conditions forming different NbN_x phases [17]. Nitrogen diffusion occurs by movement of lattice defects. Nitrogen diffuses in Nb by vacancy diffusion in both γ and δ niobium nitrides [27,28]. Therefore large concentration of nitrogen vacancies are present in these two phases.

Niobium nitrides with both δ and β phases grown by thermal nitriding in the range of 1100–1900 °C at 15×10^4 Pa were reported [17]. As samples cooled down to less than 1350 °C, the thin layer of the δ phase transformed into γ, ε and δ' phases. Lengauer et al. [29]. reported on high-temperature nitridation of Nb annealed in high-purity nitrogen at various pressures, times and temperatures below 1400 °C. Phase transformations of γ-Nb_4N_3 to δ-NbN and η-NbN to δ-NbN were observed between 1070 and 1300 °C, respectively. In their earlier work, an investigation was performed for the nitrogen pressure range of $10^3-3\times10^6$ Pa and temperature range of 1400–1800 °C [30]. The choice of nitrogen pressure is important for growth rate and homogeneity of the formed NbN_x phases [30].

Most previous works were done using the thermal diffusion method to find the equilibrium phases and the structural properties of these phases. Also, these works were done at relatively high nitrogen gas pressures to obtain different phases that show high T_c, such as δ-NbN, γ-NbN and β-Nb_2N phases. Phase diagram of Nb-N system is complex and consists of different phases. Up to now several different phase diagrams were proposed [16,29,30,35]. The α-NbN phase is the solid solution of nitrogen in niobium, which is rather less studied and not very well understood. The reaction between niobium and nitrogen is mainly dominated by diffusional transport of nitrogen. The properties of the α-NbN formed layer can be controlled by the nitrogen pressure and the temperature of the Nb substrate. Here we study the formation of the α-NbN solid solution phase by performing experiments at lower nitrogen pressures than previously reported [31]. A series of experiments were performed to investigate the formation and electronic structure of NbN_x at different temperatures in constant nitrogen pressure using the thermal diffusion method. In the present work we explore the mechanism for formation of α-NbN in the condition of reactive diffusion upon variation in temperature.

2. Experimental setup

The Nb substrates ($8\times3\times0.2$ mm^3) were etched by the buffered chemical polishing (BCP) method at the same conditions previously used [11]. The samples were kept at 600–650 °C during the baking of the experimental chamber. During chamber baking, the base pressure was in the mid 10^{-6} Pa.

No heat treatments were done before starting the nitridation of the samples. The thermal nitridation was done at different temperatures ranging from 1250 to 1500 °C for a period of 180 min. The nitrogen gas was introduced to the chamber through an ultrahigh vacuum (UHV) leak valve to reach the desired pressure in 20–30 s. For samples heated in vacuum lower than 1.3×10^{-5} Pa, no introduction of nitrogen gas into Nb was done. Tungsten wire heater-baskets were used for sample heating. The sample temperature was measured by a pyrometer (IGA 15 plus, Mikron Infrared Inc.). When the desired time for nitridation was reached, the UHV valve was opened and the power supplied to the sample heater was turned off simultaneously to allow the sample to cool down in the vacuum to room temperature before removal from the UHV chamber.

XRD measurements were done using Bruker-AXS three-circle diffractometer. A Bruker SMART APEX II instrument is equipped with graphite-monochromated CuK_α radiation and a SMART Apex II CCD detector. X-ray source of wavelength of 1.5406 Å (Cu-Kα line) is fixed and both the charge coupled device (CCD) detector (2θ) and sample (ω) are movable. The detector (2θ) is covering about 30° per image position. Three image positions were used for the experiment. In each case, the angle 2θ is the center position of the 30° CCD image, and each value is set so that the angles of incidence and diffraction are equal. Two-dimensional (2D) XRD images are recorded on diffraction patterns of each sample.

The X-ray absorption near edge structure (XANES) measurements were performed on beamline 8.2 at the Stanford Synchrotron Radiation Lightsource in the SLAC National Accelerator Laboratory. The total electron yield (TEY) mode was used for XANES measurements by measuring sample current. The current measurements were done using a low noise preamplifier (Stanford research system Model SR570). The beam flux (I_o) signal from a gold grid was used to normalize the spectra. The base pressure of the XANES chamber during the experiment was about 2.0×10^{-7} Pa.

3. Results and discussion

Fig. 1 shows the XRD of niobium nitride coatings fabricated by heating the Nb substrate at different temperatures in constant nitrogen pressure (1.3×10^{-3} Pa) for 180 min processing time. The XRD pattern of the unheated Nb substrate is also included in Fig. 1 as a reference.

XRD patterns show no clear evidence of nitridation for samples processed at temperature ranging from 1250 to 1500 °C, because the most highest XRD peaks of both Nb and α-NbN are at the same 2θ values [32,33]. For a more detail view of the XRD patterns, the 2D–XRD images

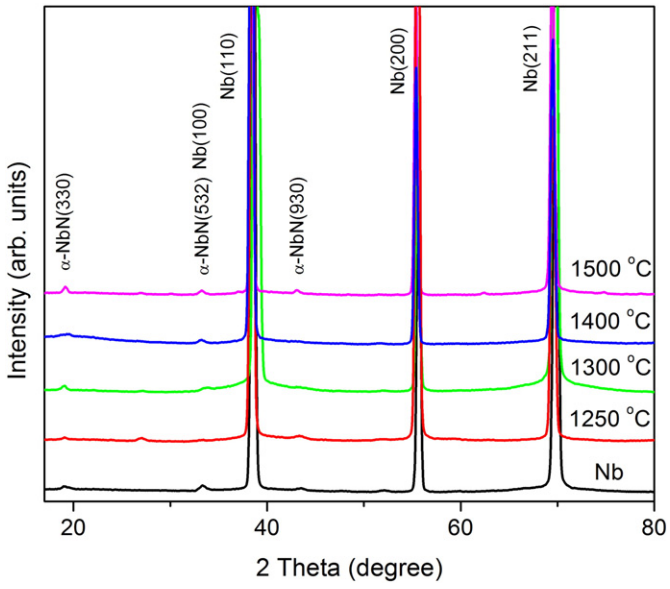


Fig. 1. XRD patterns of unheated Nb substrate and heat-treated Nb at the temperatures between 1250 and 1500 °C for 180 min in 1.3×10^{-3} Pa nitrogen background pressure.

of the samples were recorded and are shown in Fig. 2. Using 2D–XRD images makes XRD a good tool for phase identification of the crystal orientation of the samples [34]. The 2D–XRD of the Nb substrate in Fig. 2 shows a strong spot at $2\theta = 69.52°$, which is an indication of dominant orientation in Nb (211) direction. As samples were heated to 1250 °C, fine grains with strong texture were formed. The size of the grains gets smaller as the temperature increases which is indicated by the formation of spotty rings at 1500 °C.

According to the Nb-N phase diagram, diffusion of the nitrogen through the surface initially forms the bcc α-NbN phase [15,16]. In the present experiment, the maximum amount of nitrogen diffused into the Nb substrate at a temperature of 1500 °C. Therefore, at that temperature we observe the largest lattice constant.

The calculated average crystallite size using the Scherrer equation and lattice constants of the α-NbN from XRD patterns are shown in Fig. 3. The error bars in Fig. 3 represent the values of the standard deviation for calculation of different diffraction planes in XRD patterns. The obtained average lattice parameter of the highest three XRD peaks in Fig. 1 (Nb(110), Nb(200), and Nb(211)) are higher than that of the unheated Nb substrate (3.294 Å). The increase in the lattice constant with increasing nitrogen content in Nb agrees well with the result given by Taylor and Dole [35,36]. It also confirms the formation of the α-NbN phase in our samples. The lattice constant of Nb is increased due to dissolving nitrogen in niobium. It has been shown that the lattice parameter of a = 3.294 Å for pure Nb increases to 3.306 Å at 1.05 at.% nitrogen [35]. As observed in Fig. 3, if the temperature is raised, crystallite size of α-NbN increases as a result of more nitrogen dissolving in Nb. Therefore, we can conclude that nitrogen dissolves within the grains and in the grain boundaries.

The α-NbN phase content was obtained by using the integrating area under the each related XRD peaks in Fig. 1. The α-NbN phase concentration was calculated as the ratio of the sum of the intensities of the α-NbN peaks divided by the total intensities of all XRD peaks. The effect of the processing temperature on the concentration of the α-NbN is shown in Fig. 4. The solid curve in the figure shows the result of the best fit to the exponential function ($y = y_0 + A_1\, e^{x/t_1}$). This shows that, in the studied range of temperature and constant background pressure, the α-NbN phase concentration in Nb follows an exponential growth with temperature.

XANES is considered as a powerful tool to investigate the electronic and atomic structures of materials [37]. The total electron yield (TEY)

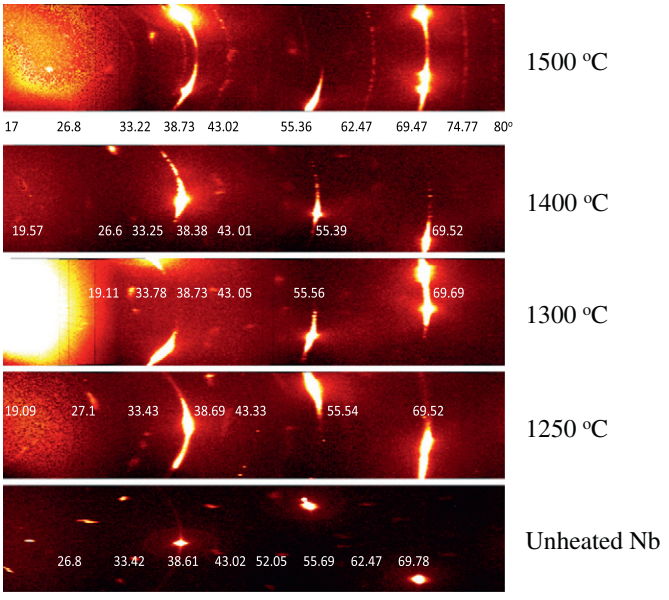


Fig. 2. 2D-XRD patterns of unheated Nb substrate and heat-treated Nb at temperatures between 1250 and 1500 °C for 180 min in1.3×10^{-3} Pa background nitrogen pressure.

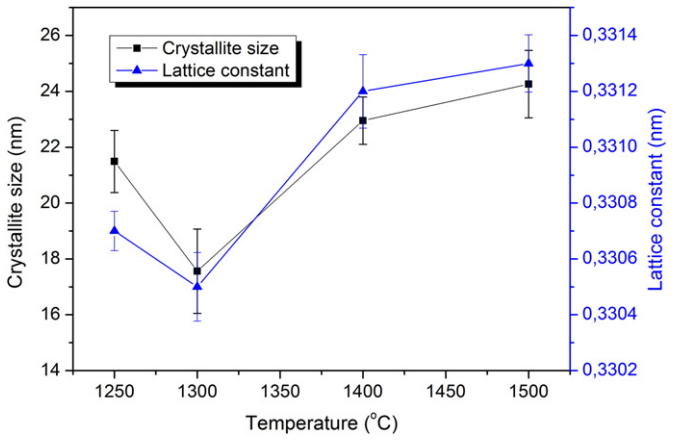


Fig. 3. Variation of mean crystallite size and lattice parameter with temperature calculated from Fig. 1.

detection is commonly used to record spectra of XANES. We used TEY mode to record the sample signal which was monitored by the drain current through the sample, and then the measured sample current was normalized to incoming photon flux. Fig. 5(a) shows XANES spectra for Nb $M_{3,2}$ edge while Fig. 5(b) is the measured branching ratio of the intensity, both as a function of heating temperature.

The Nb $M_{2,3}$ edges are attributed to the transition of Nb 3*p* electrons to unoccupied 4*d* and 5*s* states. The two peaks at about 365.5 and 380.5 eV can be assigned to the Nb $3p_{3/2}$ and $3p_{1/2}$, respectively. The peak at 365.5 eV is stronger than that at 380.5 eV. The intensity of nitrogen K-edge peak at 406.5 eV did not show any noticeable alteration with changes in the heating temperature.

The branching ratio (BR) is defined as the intensity ratio of $I(M_3)$ / $[I(M_2) + I(M_3)]$ where $I(M_3)$ and $I(M_2)$ are the measured area under the M_3 ($j = 3/2$) and M_2 ($j = 1/2$) peaks, respectively, and which is proportional to the oscillator strength of the 3*p*–4*d* and/or 3*p*–5*s* states spin–orbit interactions. The BR is changed significantly from 0.615 to 0.650 as the processing temperature was increased from 1250 to 1500 °C. Fig. 4(b) shows that the electronic structure changes a little for samples processed above 1400 °C compared to samples processed below that temperature. For samples processed at 1400 and 1500 °C, the branching ratio was almost similar. This result is consistent with the findings in Fig. 3 that the lattice parameter did not change much after 1400 °C. The change in the BR intensity indicates a changes in

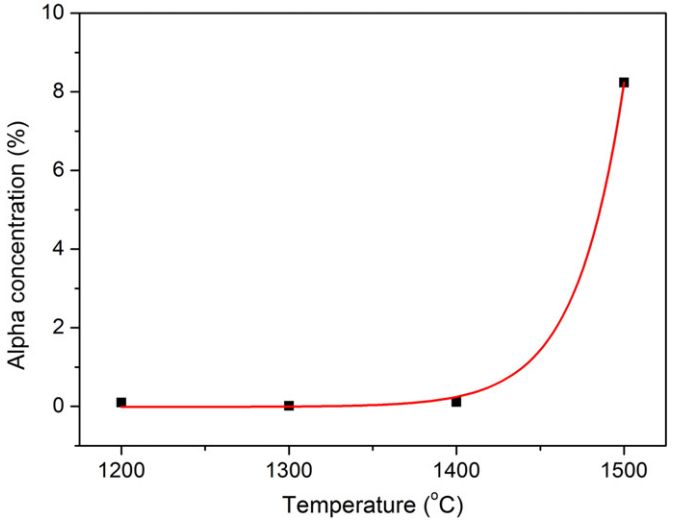


Fig. 4. Influence of the heat treatment on concentration of the α-NbN cubic phase. The solid line is curve-fit to experimental data.

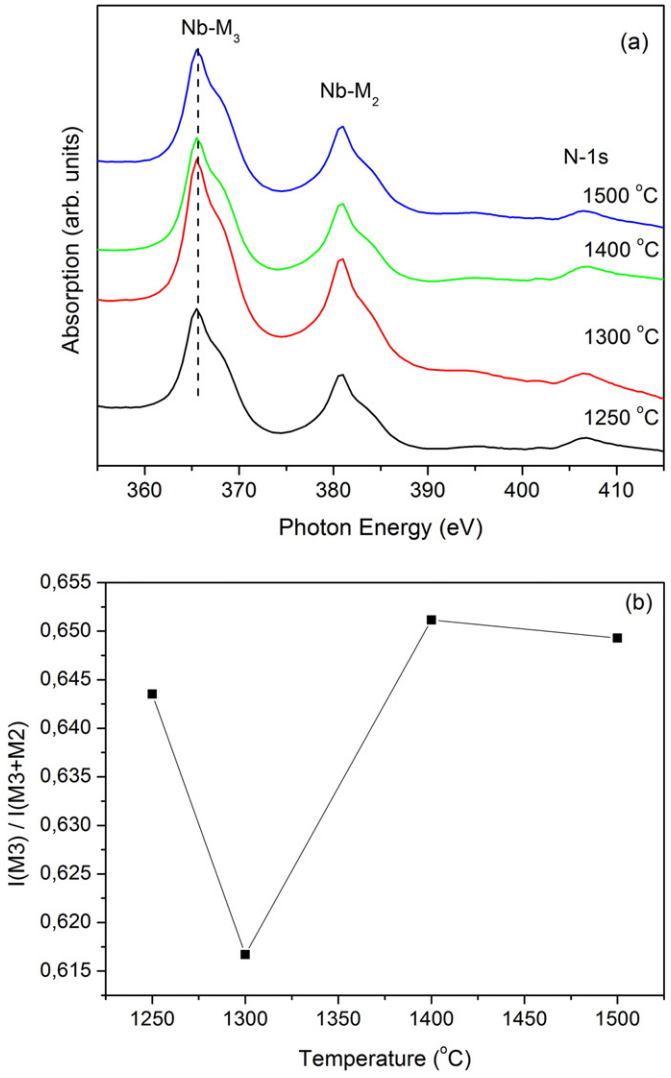


Fig. 5. XANES spectra of NbN_x at the Nb $M_{3,2}$ edge region as a function of processing temperatures (a) and branching ratio of the peak intensities at the $M_{3,2}$-edge as a function of processing temperature. The drawn line serves only guide the eye (b).

the coordination of the Nb and N atom with increasing α-NbN phase concentration. Furthermore, the BR is found to be strongly dependent on the local chemical environment. This can be explained by higher processing temperature resulting in more nitrogen incorporation into niobium which increases hybridization between the Nb 4*d* and N 2*p* levels. Larger covalent contribution to the Nb–N bonding enhances the strong 3*p*-4*d* Coulomb interaction leading to strong BR. Higher temperature samples resulted in higher electron-core-hole interaction and the number of *d* final states available.

4. Conclusion

Thermal diffusion of nitrogen into Nb forming the α-NbN phase was studied. The samples were heated for 180 min at different temperatures (1250–1500 °C) and constant 1.3×10^{-3} Pa nitrogen pressure. In 2D-XRD images show the formation α-NbN grains. From the ring shape, the grains become smaller as the temperature is increased to 1500 °C. This observation is consistent with the crystallite size calculated using the Scherrer relation. The average crystallite size decreases from ~21.4 nm at 1250 °C to ~17.6 nm at 1500 °C. The calculated lattice constants from the three Nb peaks with highest intensity showed transformation from decreasing to increasing as the temperature is raised from 1250 to 1500 °C. The present results indicate that the most favorable temperature for the formation of the α-NbN phase by heat treatment is 1400–1500 °C at 1.3×10^{-3} Pa nitrogen pressure. Furthermore, from XANES measurements for the Nb $M_{2,3}$ edge, we found that at the higher processing temperature of 1500 °C, the number of *d* holes increased, and as a result the spin–orbit interaction also increased yielding higher branching ratio values at the M edge. We observed only the formation of α-NbN phase in the studied temperature and background nitrogen pressure range. Different gas pressure and temperature ranges results in the formation of different NbN_x phases and morphologies [31].

The amount of dissolved nitrogen in niobium *x* in at.% can be expressed by the equation [35]:

$$x = A\sqrt{P_{N2}}\exp(\Delta H_N/RT) \quad (1)$$

where *A* is constant, P_{N2} is the pressure of nitrogen, ΔH_N is the heat of solution of nitrogen in the α-NbN phase, *R* is the gas constant and *T* is temperature. The equilibrium concentration of nitrogen in niobium is related to the processing temperature and background nitrogen gas pressure. A summary of the different Nb-N phases for different nitrogen incorporation in Nb is given in Ref. [35]. It was revealed that only the α-NbN is formed for our experimental conditions. The XRD patterns obtained clearly indicate that only the α-NbN phase is present and no transformation to another NbN_x phases is observed. The α-NbN phase is identified by its body centered cubic (bcc) structure, similar to Nb but with increase lattice parameter due to nitrogen incorporation. For the experimental conditions in the present study, the XRD patterns did not show the formation of the hexagonal closed packed (hcp) Nb_2N, the tetragonal NbN, or any of the other known Nb-N structures.

Acknowledgments

A. H. F. was supported by a scholarship from the Egyptian Ministry of Higher Education and a Jefferson Lab scholarship funded by the Department of Energy Office of Nuclear Physics ARRA-NPQ project at Jefferson Lab under the U.S. DOE Contract No. DE-AC05-06OR23177. The authors are grateful to the Stanford Synchrotron Radiation Light source (SSRL), California, USA, for providing synchrotron-based XAS facility. Use of SSRL source is supported by the US Department of Energy, Office of Basic Energy Sciences, under Contract No. DEAC02-76SF00515. Support of DOE Cooperative Research Program for SESAME project is acknowledged by A.H.F., O.M.O. and Y.U.

References

[1] M. Radparvar, Cryogenics 35 (1995) 535–540.
[2] M. Lucci, H.N. Thanh, I. Davoli, Superlattice. Microst. 43 (2008) 518–523.
[3] R. Sobolewski, A. Verevkin, G.N. Gol'tsman, A. Lipatov, K. Wilsher, IEEE Trans. Appl. Supercond. 13 (2003) 1151–1157.
[4] S. Miki, Y. Uzawa, A. Kawakami, Z. Wang, Electron. Commun. Jpn. (Part II: Electronics) 85 (2002) 77–83.
[5] A.D. Semenov, H.W. Hubers, IEEE Trans. Appl. Supercond. 11 (2001) 196–199.
[6] D. Bekermann, D. Barreca, A. Gasparotto, H.W. Becker, R.A. Fischer, A. Devi, Surf. Coat. Technol. 204 (2009) 404–409.
[7] B. Abdo, E. Arbel-Segev, O. Shtempluck, E. Buks, IEEE Trans. Appl. Supercond. 16 (2006) 1976–1987.
[8] E.J. Cukauskas, W.L. Carter, S.B. Qadri, J. Appl. Phys. 57 (1985) 2538–2542.
[9] Y. Gotoh, M. Nagao, T. Ura, H. Tsuji, J. Ishikawa, Nucl. Instrum. Methods Phys. Res., Sect. B 148 (1999) 925–929.
[10] A.H. Farha, A.O. Er, Y. Ufuktepe, G. Myneni, H.E. Elsayed-Ali, Surf. Coat. Technol. 206 (2011) 1168–1174.
[11] A.H. Farha, A.O. Er, Y. Ufuktepe, H.E. Elsayed-Ali, Mater. Chem. Phys. 132 (2012) 667–672.
[12] R.E.d. Lamaestre, P. Odier, J.-C. Villegier, Appl. Phys. Lett. 91 (2007) 232501–232503.
[13] M.A. Al Mamun, A.H. Farha, Y. Ufuktepe, H.E. Elsayed-Ali, A.A. Elmustafa, J. Mater. Res. 27 (2012) 1725–1731.
[14] M.A. Mamun, A.H. Farha, A.O. Er, Y. Ufuktepe, D. Gu, H.E. Elsayed-Ali, A.A. Elmustafa, Appl. Surf. Sci. 258 (2012) 4308–4313.
[15] H. Bauer, J. Low Temp. Phys. 24 (1976) 219–227.
[16] G. Brauer, J. Less-Common Met. 2 (1960) 131–137.
[17] R. Musenich, P. Fabbricatore, G. Gemme, R. Parodi, M. Viviani, B. Zhang, V. Buscaglia, C. Bottino, J. Alloys Compd. 209 (1994) 319–328.
[18] A.V. Linde, R.M. Marin-Ayral, D. Granier, F. Bosc-Rouessac, V.V. Grachev, Mater. Res. Bull. 44 (2009) 1025–1030.

[19] A.V. Linde, V.V. Grachev, R.M. Marin-Ayral, Chem. Eng. J. 155 (2009) 542–547.
[20] V. Buscaglia, F. Caracciolo, M. Ferretti, M. Minguzzi, R. Musenich, J. Alloys Compd. 266 (1998) 201–206.
[21] C. Angelkort, H. Lewalter, P. Warbichler, F. Hofer, W. Bock, B.O. Kolbesen, Spectrochim. Acta A Mol. Biomol. Spectrosc. 57 (2001) 2077–2089.
[22] A. Berendes, O. Brunkahl, C. Angelkort, W. Bock, F. Hofer, P. Warbichler, B.O. Kolbesen, Anal. Bioanal. Chem. 379 (2004) 554–567.
[23] C. Benvenuti, P. Chiggiato, L. Parrini, R. Russo, Nucl. Instrum. Methods Phys. Res., Sect. A 336 (1993) 16–22.
[24] P. Fabbricatore, G. Gemme, R. Musenich, R. Parodi, M. Viviani, B. Zhang, V. Buscaglia, IEEE Trans. Appl. Supercond. 3 (1993) 1761–1764.
[25] M. Pham Tu, K. Mbaye, L. Wartski, J. Halbritter, J. Appl. Phys. 63 (1988) 4586–4590.
[26] G. Gemme, P. Fabbricatore, R. Musenich, R. Parodi, T. Rossi, M. Viviani, B. Zhang, J. Appl. Phys. 77 (1995) 257–264.
[27] S.J. Kim, H.F. Franzen, J. Less-Common Met. 143 (1988) 339–343.
[28] G. Heger, O. Baumgartner, J. Phys. C Solid State Phys. 13 (1980) 5833.
[29] W. Lengauer, M. Bohn, B. Wollein, K. Lisak, Acta Mater. 48 (2000) 2633–2638.
[30] M. Joguet, W. Lengauer, M. Bohn, J. Bauer, J. Alloys Compd. 269 (1998) 233–237.
[31] Y. Ufuktepe, A.H. Farha, S.-i. Kimura, T. Hajiri, F. Karadağ, M.A. Al Mamun, A.A. Elmustafa, G. Myneni, H.E. Elsayed-Ali, Mater. Chem. Phys. 141 (2013) 393–400.
[32] I.C.f.D. data, Powder Diffraction File 00-035-0789, 2004.
[33] I.C.f.D. data, Powder Diffraction File 00-043-1420, 2004.
[34] B.B. He, Two-dimensional X-Ray Diffraction, Wiley-Interscience, Hoboken, USA, 2009.
[35] A. Taylor, N.J. Doyle, J. Less-Common Met. 13 (1967) 399–412.
[36] A. Taylor, N.J. Doyle, J. Less-Common Met. 13 (1967) 413–430.
[37] N. Schonberg, Acta Chem. Scand. 8 (1954) 208–212.